Supplementary Materials for

Future Antarctic bed topography and its implications for ice sheet dynamics

by S. Adhikari, E. R. Ivins, E. Larour, H. Seroussi, M. Morlighem and S. Nowicki

May 12, 2014

Introduction

In this document, we present seven figures that supplement to the main text. Sample results from the benchmark experiments [Ivins and James, 1999] are plotted in Fig. S1. Effects of mesh resolution on solution accuracy are also illustrated. In Figs. S2 and S3, we present examples of the past and future DIHs, respectively. The lone ice loading history considered in our calculations is obtained from Ivins et al. [2013]. As for the future, we have four individual sets of the ice load change predicted by the SeaRISE participating ice sheet models [Bindschadler et al., 2013; Nowicki et al., 2013] under the R8 scenario.

We show in Figs. S4–S5 the bed uplift predictions for individual future ice loading, combined with the consideration of a lone spin-up loading history, at years 2100 and 2500 AD. Model-average solutions for future bed uplift rate and associated standard deviations are shown in Fig. S6. In Fig. S7, we isolate the contribution of the past and future ice loading (model-average) to the predicted GIA uplifts at year 2500 AD. Two independent calculations suggest that the role of the future ice loading dominates the final GIA solutions. Finally, in Fig. S8, we plot 2744 ice flowlines that are tracked to quantify the GL migration.

References

Bindschadler, R., Nowicki, S., Abe-Ouchi, A., Aschwanden, A., Choi, H., Fastook, J., Granzow, G., Greve, R., Gutowski, G., Herzfeld, U., Jackson, C., Johnson, J., Khroulev, C., Levermann, A., Lipscomb, W., Martin, M., Morlighem, M., Parizek, B., Pollard, D., Price, S., Ren, D., Saito, F., Sato, T., Seddik, H., Seroussi, H., Takahashi, F., Walker, R., and Wang, W.: Ice-Sheet Model Sensitivities to Environmental Forcing and Their Use in Projecting Future Sea-Level (The SeaRISE Project), J. Glaciol., 59, 195–224, doi:10.3189/2013JoG12J125, 2013.

Ivins, E. R. and James, T. S.: Simple models for late Holocene and present-day Patagonian glacier fluctuations and predictions of a geodetically detectable isostatic response, Geophys. J. Int., 138, 601–624, doi:10.1046/j.1365-246x.1999.00899.x, 1999.

Ivins, E. R., James, T. S., Wahr, J., O. Schrama, E. J., Landerer, F. W., and Simon, K. M.: Antarctic contribution to sea level rise observed by GRACE with improved GIA correction, J. Geophys. Res., 118, 3126–3141, doi:10.1002/jgrb.50208, 2013.

Nowicki, S., Bindschadler, R., Abe-Ouchi, A., Aschwanden, A., Bueler, E., Choi, H., Fastook, J., Granzow, G., Greve, R., Gutowski, G., Herzfeld, U., Jackson, C., Johnson, J., Khroulev, C., Larour, E., Levermann, A., Lipscomb, W., Martin, M., Morlighem, M., Parizek, B., Pollard, D., Price, S., Ren, D., Rignot, E., Saito, F., Sato, T., Seddik, H., Seroussi, H., Takahashi, K., Walker, R., and Wang, W.: Insights into spatial sensitivities of ice mass response to environmental change from the SeaRISE ice sheet modeling project I: Antarctica, J. Geophys. Res., 118, 1–23, doi:10.1002/jgrf.20081, 2013.

Rignot, E., Mouginot, J., and Scheuchl, B.: Ice Flow of the Antarctic Ice Sheet, Science, 333, 1427–1430, doi:10.1126/science.1208336, 2011.

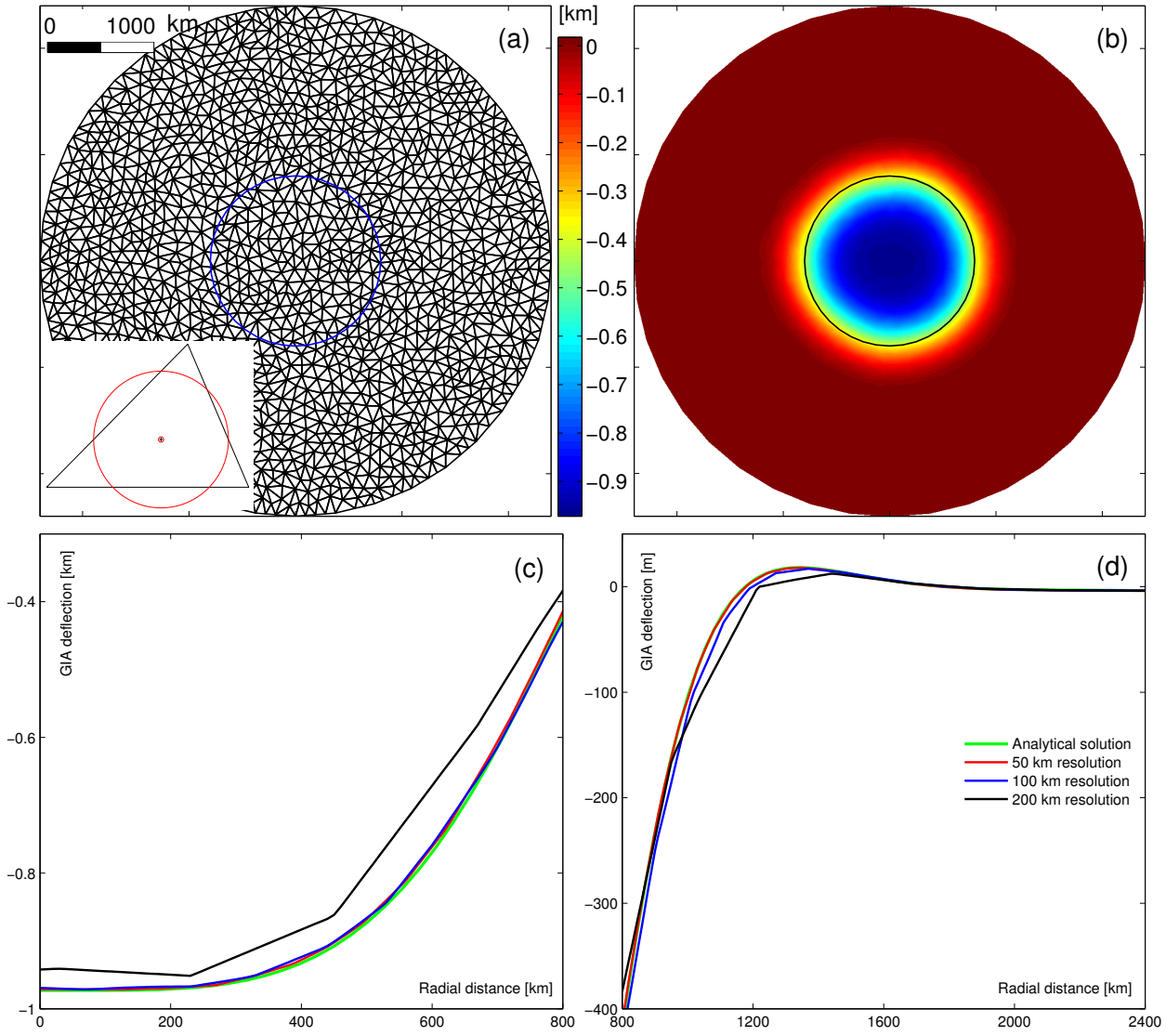

Figure S1: Example benchmark experiment. A round ice sheet, with a radius of 800 km (notice blue and black circles in Figs. S1a and S1b, respectively) and a uniform ice thickness of 3 km, rests on the initial flat bed for sufficiently long time so that the steady-state solid Earth response is attained. This resembles one of the benchmark experiments considered by Ivins and James [1999] (see their Fig. A2c). Other parameters include: lithosphere thickness (100 km); material density for ice, lithosphere and mantle (1000, 3320 and 3340 $\mathrm{kg\,m^{-3}}$, respectively); shear modulus of elasticity for lithosphere and mantle (67 and 145 GPa, respectively); and mantle viscosity (10^{21} Pa s). **(a)** A finite-element discretization of the domain including farfield, with maximum element size of 100 km. Inset shows a typical mesh element (triangle) whose gravity centre and area characterize the position and size of the disc load (circle). **(b)** Corresponding steady-state GIA solution. Effects of mesh resolution on the GIA solutions **(c)** underneath the ice sheet, and **(d)** in the farfield.

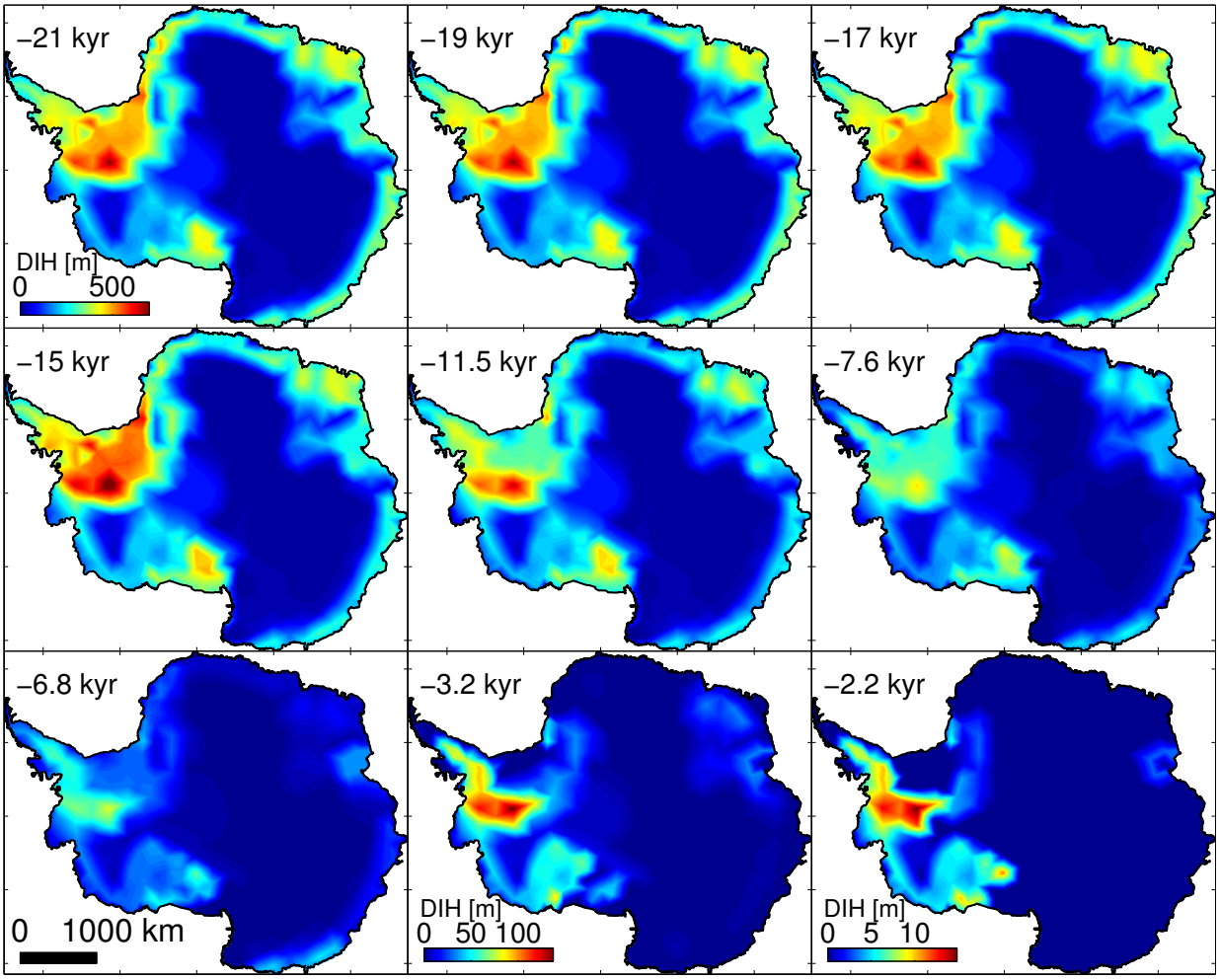

Figure S2: Inferred ice loading history since the LGM. The DIHs, $\Delta h(x, y, t)$ in meters, shown for nine time stamps in the past are obtained from Ivins et al. [2013]. Note that we assume $\Delta h(x, y, -102) = \Delta h(x, y, -1) = 0$ meters as explained in the main text. For ease of comparison, same color scale is used except for $t = -3.2$ and -2.2 kyr.

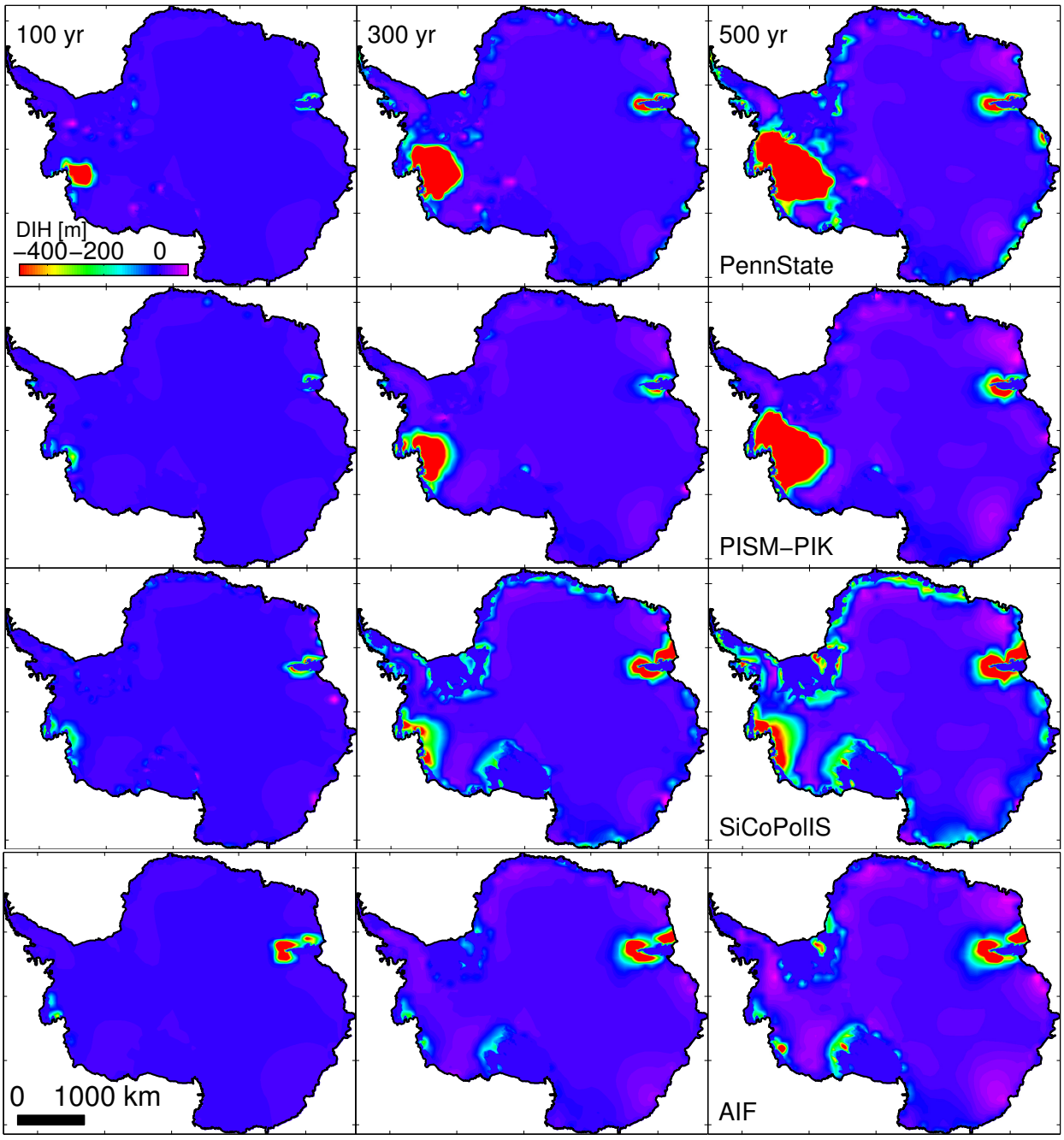

Figure S3: Examples of predicted ice load change for the future. Four rows of the figure respectively depict the future ice loading obtained from the PennState, PISM-PIK, SiCoPolIS, and AIF ice sheet model simulations. For each model, three columns of the figure respectively depict the DIHs at $t = 100$, 300 and 500 years. We use the same color scale for ease of comparison. However, note that PennState and PISM-PIK models predict ice loss (some times in the future) by more than 3 km around the Amundsen Sector. SiCoPolIS and AIF predict moderate mass loss; about 1.5 km, for example, around the Amundsen Sector (only SiCoPolIS) and Amery Ice Shelf.

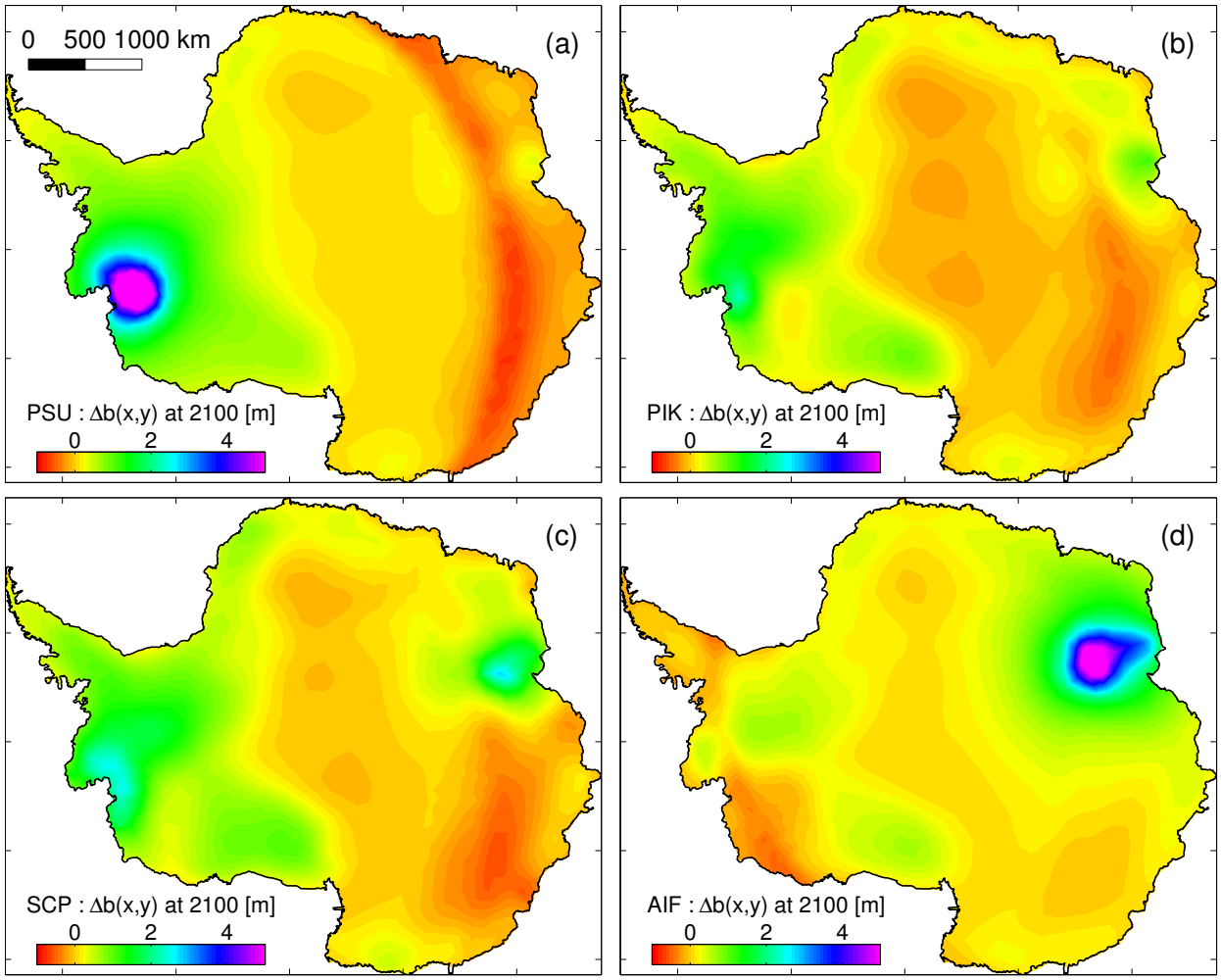

Figure S4: Model predictions for the bed uplift at 2100 AD. The GIA solutions associated with the future ice loading obtained from the **(a)** PennState, **(b)** PISM-PIK, **(c)** SiCoPolIS, and **(d)** AIF ice sheet models. Same color scale is used for ease of comparison. Note that the model-average GIA solutions and the standard deviations are respectively shown in Figs. 3a and 3c (main text).

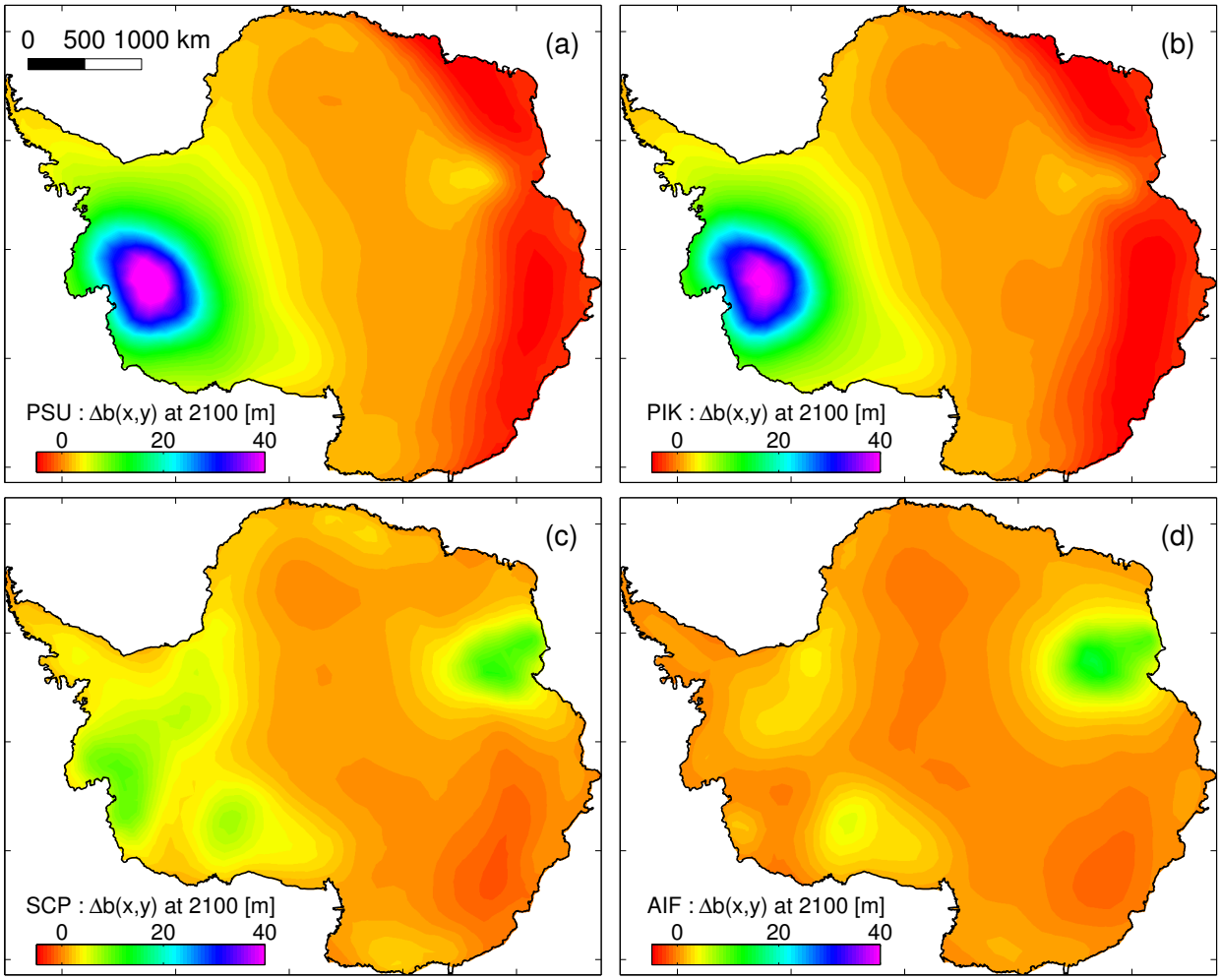

Figure S5: Model predictions for the bed uplift at 2500 AD. The GIA solutions associated with the future ice loading obtained from the **(a)** PennState, **(b)** PISM-PIK, **(c)** SiCoPolIS, and **(d)** AIF ice sheet models. Same color scale is used for ease of comparison. Note that the model-average GIA solutions and the standard deviations are respectively shown in Figs. 3b and 3d (main text).

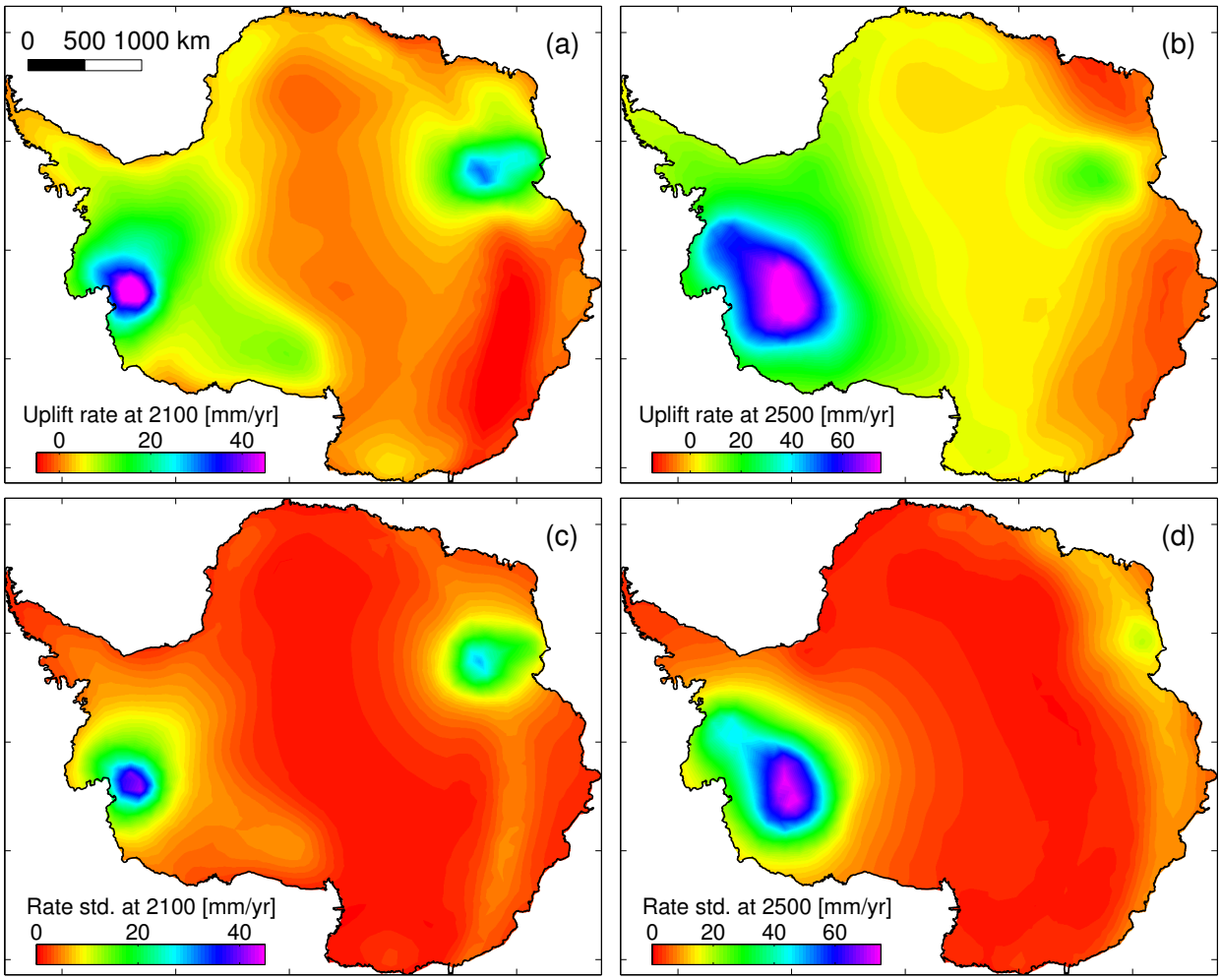

Figure S6: Estimates of the future Antarctic bed uplift rate. Model-average predictions for bed uplift rate at **(a)** 2100 AD and **(b)** 2500 AD under the R8 scenario. Associated standard deviations are shown in subplots **(c)** and **(d)**, respectively. See Fig. 3 of the main text for corresponding solutions for the future bed uplift.

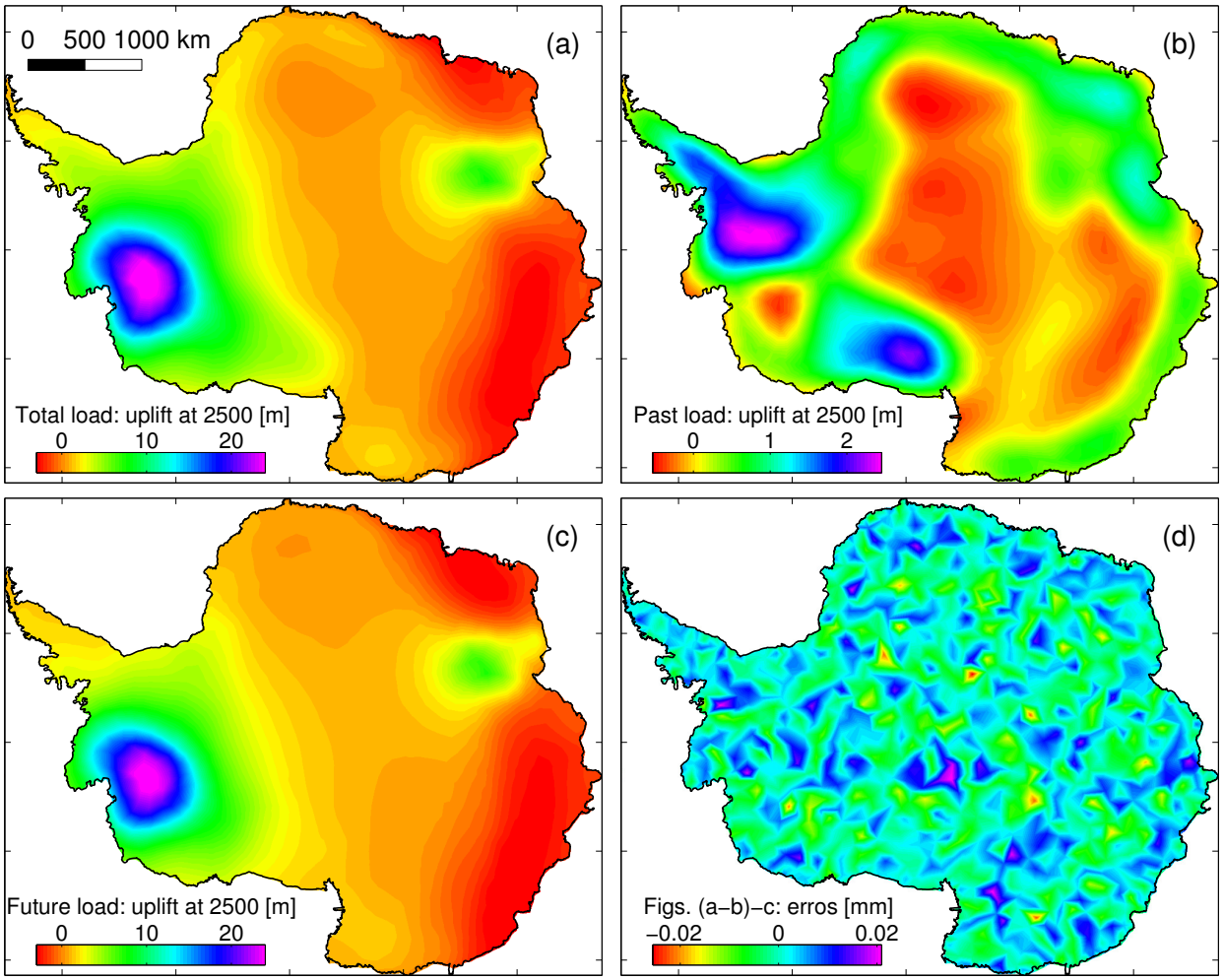

Figure S7: Contribution of the past and future ice loading to the GIA solutions at 2500 AD. **(a)** Predictions of the GIA uplift obtained by averaging the solutions shown in Fig. S4 (same as Fig. 3a in the main text). **(b)** GIA solutions due to the past loading alone, assuming that the present-day AIS remains as is in the future. **(c)** GIA solutions (model-average) due to the future ice loading alone, assuming that the past AIS used to have the same configuration as present for sufficiently long time. An alternative solution equivalent to Fig. S7c may be obtained by subtracting Fig. S7b from Fig. S7a. **(d)** Difference between the alternative solution and the one depicted in Fig. S7c. Minor errors imply that the principle of linear superposition holds. Note that we use different color scale in Fig. S7a–c in order to illustrate the spatial distributions.

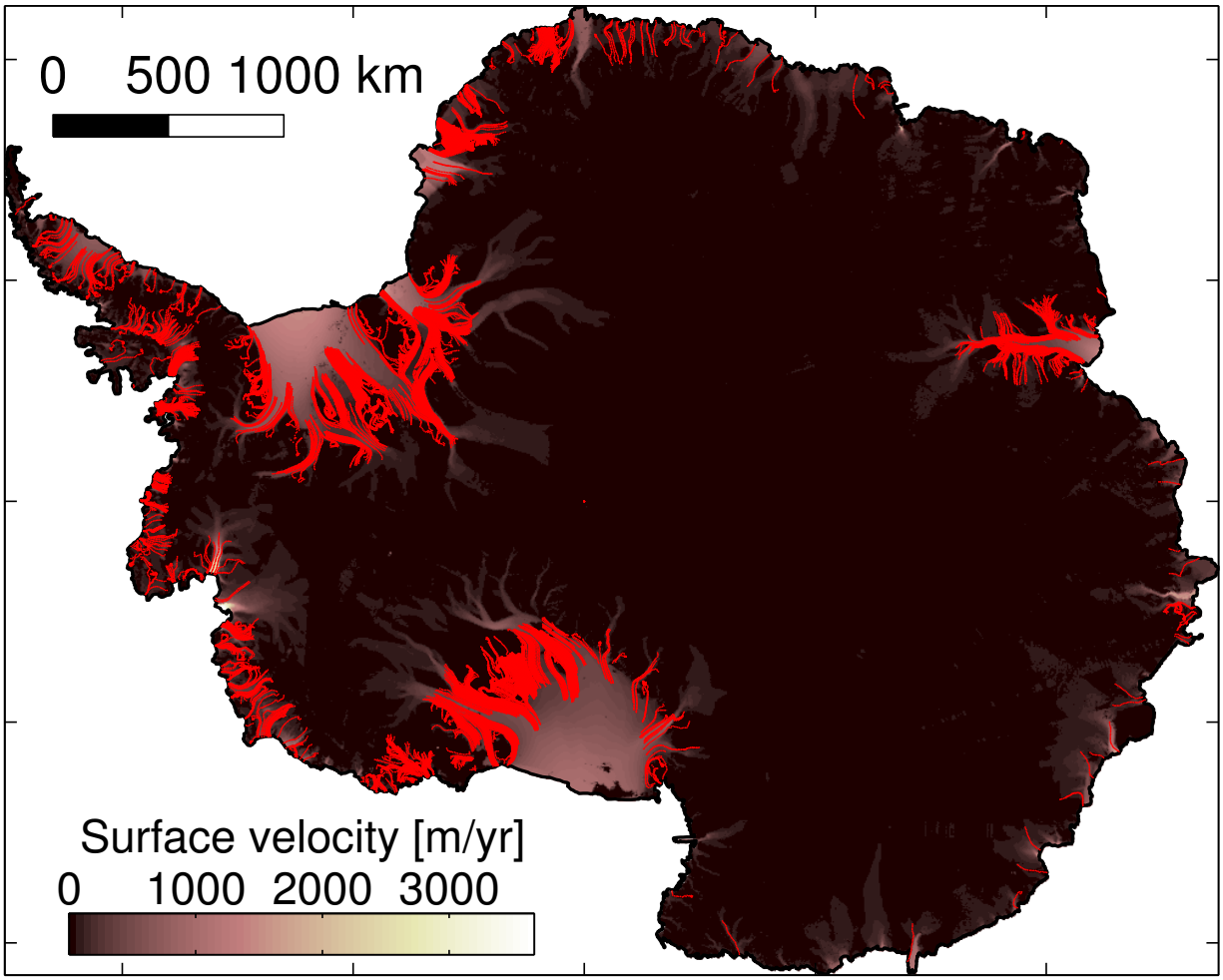

Figure S8: Location of 2744 ice flowlines (red lines). These flowlines are tracked to quantify the GL migration (cf. Fig. 7 in the main text). The background color shows the present-day measured ice surface velocity [Rignot et al., 2011].